Journal of Materials Chemistry A

Accepted Manuscript

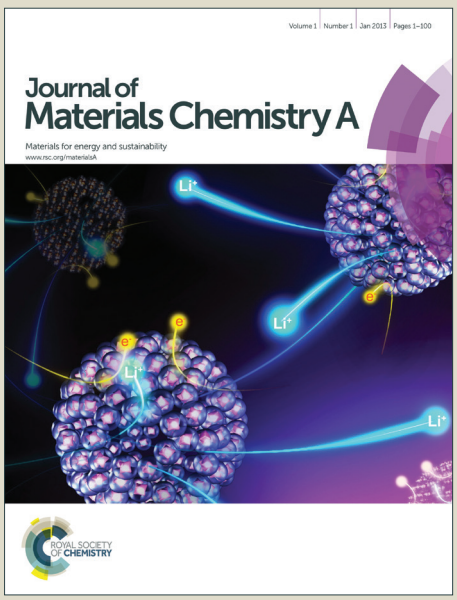

ROYAL SOCIETY OF CHEMISTRY

www.rsc.org/materialsA

Ni-Co sulfides nanowires on nickel foam with ultrahigh capacitance for asymmetric supercapacitor

Yanhong Li,[a] Liujun Cao,[b] Lei Qiao,[b] Ming Zhou,[b] Yang Yang,[b] Peng Xiao,[*a,b] and Yunhuai Zhang[*b]

[a] *College of Physics, Chongqing University, Chongqing 400044, China*

[b] *College of Chemical Engineering, Chongqing University, Chongqing 400044, China*

[*] Corresponding author. Tel-86-23-65102031

Email address: xiaopeng@cqu.edu.cn

xp2031@163.com

Abstract

In this paper we firstly synthesize well aligned Ni-Co sulfides nanowire arrays (NWAs) with Ni-Co molar ratio of 1 : 1 on 3D nickel foam by a facile two-step hydrothermal method. Owing to the low electronegativity of sulfur, Ni-Co sulfides NWAs exhibit more flexible structure and much higher conductivity compared with Ni-Co oxides NWAs when used as active material in supercapacitor. The electrochemistry tests show that this self-supported electrode is able to deliver ultrahigh specific capacitance (2415 F g^{-1} and 1176 F g^{-1} at current density of 2.5 mA cm^{-2} and 30 mA cm^{-2}, respectively), together with a considerable areal capacitance (6.0 F cm^{-2} and 2.94 F cm^{-2} at current density of 2.5 mA cm^{-2} and 30 mA cm^{-2}, respectively), and good rate capability. More importantly, the asymmetric supercapacitor, composed of Ni-Co sulfides NWAs as positive electrode and activated carbon as negative electrode, reaches up to an energy density of 25 Wh kg^{-1} and power density of 3.57 kW kg^{-1} under the cell voltage of 1.8 V. Furthermore, the two assembled supercapacitors in series can power a 3 mm diameter red (2.0 V, 20 mA) round light-emitting diode (LED) indicator for more than 30 minutes after charging separately for a total time of 6 min. The superior electrochemistry capacity demonstrates that the self-standing Ni-Co sulfides nanowires arrays are promising for high-performance supercapacitor applications.

Introduction

Electrochemical capacitors, also known as supercapacitors, have attracted intense attention due to their high power density, fast charge-discharge process, long cycle life and are widely used in many practical applications.[1,2] Ni-Co oxides composites, also known as ternary metal oxides, have excited great interest in recent years because of their high-performance in supercapacitors. Owing to the coupling of two metal species, this material could render the composites with rich redox reactions and improved electronic conductivity, which are beneficial to electrochemical applications.[3-5] Different shapes and structures of Ni-Co oxides, such as nanowires,[6] porous aerogels,[4] urchin-like structures[7,8] and various nanostructures on conductive substrates[9-13] have been reported. Compared with nanostructure powders, the Ni-Co oxides nanostructures fabricated on conductive substrates demonstrate much better pseudocapacitive performance since these binder and conductive-agent-free electrodes can ensure the more efficient ion diffusion and faster electron transport.[10,11,14-16] In particular, the tunable compositions in the Ni-Co oxides provide vast opportunities to manipulate the crystal structure and its physical/chemical properties. For example, if Co/Ni ratio is fixed at 2 : 1, a spinel crystal structure $NiCo_2O_4$ is expected, while if Co/Ni co-exists in any molar ratio, a NaCl-type structure $Ni_{1-x}Co_xO$ is usually prepared.[17] Our research showed that when the Ni-Co

molar ratio was fixed at 1 : 1, the Ni-Co oxides composite presented the best electrochemical performance.[18] Although the ternary Ni-Co oxides have been intensely researched recently, it still needs the further study to explore and develop the performance of these materials by effective routes in order to achieve high-quality electrode materials for supercapacitor applications.

Similar to the oxides mentioned above, Ni-Co sulfides are also electrochemically active as electrode materials for supercapacitors and other applications.[19,20] In comparison to single phase of metal sulfides, these ternary metal sulfides exhibit higher specific capacitance due to the synergy effect of the two metallic cations. In particular, it is found that Ni-Co sulfides have much lower optical band gap energy and much higher conductivity compared to Ni-Co oxides.[21] The substitution of oxygen with sulfur might create a more flexible structure because the electronegativity of sulfur is lower than that of oxygen, which prevents the disintegration of the structure by the elongation between layers and makes it easy for electrons to transport in the structure.[22] To date, most of successful attempts are focused on fabrications of different nanostructure powders of ternary metal sulfides $NiCo_2S_4$, such as urchin-like structures,[21] porous nanotubes[23] and nanosheets on graphene.[24] Very few research investigates Ni-Co sulfides with different Ni-Co molar ratio and its fabrication of free standing electrode structure.

Herein, we report the interesting formation of Ni-Co sulfides nanowires arrays (NWAs) with Ni/Co molar ratio of 1 : 1 and their derived free standing structure as intriguing self-supported electrodes for ECs. The Ni-Co sulfides NWAs were

fabricated through S^{2-} ion exchange[21,25-27] using our previously synthesized Ni-Co oxides NWAs as precursor. The electrochemistry tests showed that this self-supported electrode was able to deliver ultrahigh specific capacitance (2415 F g^{-1} and 1176 F g^{-1} at current density of 2.5 mA cm^{-2} and 30 mA cm^{-2}, respectively). To further evaluate the practical application of Ni-Co sulfides, an asymmetric supercapacitor was fabricated. The asymmetric structure can raise the cell voltage and thereby boost the energy density more effectively by providing a wider operating potential window than symmetric ones. For demonstration of principle, we use the Ni-Co sulfides NWAs for the battery-like Faradic electrode and commercial activated carbon for the double layered capacitive electrode to compose the asymmetric cell, and this has extended the cell voltage to 1.8 V in an aqueous electrolyte, resulting in high energy density (25 Wh kg^{-1} at power density of 447 W kg^{-1}) and high power density (3.57 kW kg^{-1} at energy density of 17.8 Wh kg^{-1}).

Experimental

Preparation of Ni-Co oxides NWAs

Ni-Co oxides NWAs were prepared by a facile hydrothermal synthesis method as follows: clean nickel foam substrate was transferred into a Teflon-lined stainless autoclave (50 ml) with 20 ml distilled water and 20 ml absolute ethanol containing 1 mmol $Co(NO_3)_2 \cdot 6H_2O$, 1 mmol $Ni(NO_3)_2 \cdot 6H_2O$ and 10 mmol urea. After 6 h growth at 95 ℃, the Teflon-lined stainless autoclave was cooled down to the room temperature naturally. Then the samples were washed with distilled water and dried

naturally. Finally, they were annealed in N_2 atmosphere at 300 ℃ for 3 h.

Preparation of Ni-Co sulfides NWAs

Typically, 1 mmol $Na_2S·12H_2O$ was dissolved in 30 ml distilled water to form homogeneous solution. Then the as-prepared Ni-Co oxides NWAs above were converted to Ni-Co sulfides NWAs by transferring it and Na_2S solution to a closed bottle, which was maintained at 90 ℃ for 12 h. The final product was rinsed with distilled water and dried in vacuum at 60 ℃ for 2 h. The average mass loading of the final product was approximately 2.5 mg cm^{-2}, carefully weighted after calcination treatment.

Fabrication of the asymmetric supercapacitor

To construct an asymmetric electrochemical capacitor, the Ni-Co sulfides NWAs were used for the positive electrode and the commercial activated carbon (AC) was used as the negative electrode. The mass ratio between the positive and negative electrode was obtained based on the following equation: $\frac{m_+}{m_-} = \frac{C_- \times \Delta E_-}{C_+ \times \Delta E_+}$.[28] The negative electrode was prepared by mixing active carbon, acetylene black and 60 wt% PTFE in a 8 : 1 : 1 mass ratio, which was then pressed onto nickel foam and dried overnight. The asymmetric electrochemical capacitors were separated by a glass fiber filter paper and 1 M KOH aqueous solution was used as electrolyte.

Characterizations and electrochemical measurements

The morphologies and structures of samples were characterized by field-emission

scanning electron microscopy (FESEM, FEI, Inspector F50) equipped with an energy-dispersive X-ray spectroscopy detector (EDS), transmission electron microscopy (TEM, Tecnai G2 F20 U-TWIN), X-ray diffraction (XRD, shimadzu 2D-3AX, Cu Kα radiation, λ=1.5418 Å) and energy-dispersive X-ray spectrometer (XPS, ESCALAB 250 Thermo Fisher Scientific). Nitrogen adsorption-desorption measurements were performed on Micromeritics ASAP 2020. All the three-electrode electrochemical measurements were carried out at ambient temperature in 1 M KOH aqueous solution as the electrolyte with a Pt foil and Ag/AgCl (saturated KCl) electrode used as counter electrode and reference electrode, respectively. For comparison, a nickel foam under the same pretreatment and the prepared Ni-Co oxides and sulfides NWAs grown on nickel foam (1 cm × 1 cm) were directly used as working electrode independently. All potentials were referred to the reference electrode. The electrochemical performances of the samples were performed on a CHI66D (Chenhua, Shanghai) workstation for cyclic voltammetry (CV), galvanostatic charge/discharge measurements and electrochemical impedance spectroscopy (EIS) tests. The specific capacitance (F g^{-1}) and the areal capacitance (F cm^{-2}) in three-electrode configuration are calculated from the discharge curves according to the following equation: $C = \frac{It}{m\Delta V}$ and $C_a = \frac{It}{S\Delta V}$, where I, t, m, S and ΔV are designated as discharge current density, the total discharge time, mass of active materials, the geometrical area of the electrode and the discharge potential range, respectively. The cyclic voltammetry and galvanostatic charge-discharge tests of the asymmetric electrochemical capacitors were performed in a two-electrode cell. The

specific capacitance (F g^{-1}), energy density (Wh kg^{-1}) and power density (kW kg^{-1}) of the device are calculated from galvanostatic charge-discharge curves according to the following equations:[29] $C = \frac{It}{mV}$, $E = \frac{CV^2}{2}$, $P = \frac{E}{t}$, where C, V, I, m and t is the capacitance of the asymmetric supercapacitor, the operating voltage window, the discharge current density, total mass loading of both negative and positive electrodes and the discharge time.

Results and discussion

Morphology and structure characterizations

Fig. 1a illustrates the two-step environmentally benign growth scheme of the Ni-Co sulfides nanowires on nickel foam. First is the hydrothermal growth of Ni-Co oxides NWAs with a Ni/Co molar ratio of 1 : 1 on nickel foam substrate serving as the backbone. Second is the formation of Ni-Co sulfides NWAs by subsequent ion-exchange reaction between O^{2-} and S^{2-} for 12 hours. The color of the sample changed from golden to black after ion-exchange reaction. The morphologies of Ni-Co sulfides structures are examined by FESEM as shown in Fig. 1c and d. It can be observed that Ni-Co sulfides NWAs with high density are grown uniformly on macroporous nickel foam, forming a 3D hierarchical structure and the nanowires lie perpendicular to the substrate and are separated apart adequately. The overall alignment results in better charge transfer kinetics, as well as easier ion diffusion without the necessity of binder blocks. The sharp tips tend to connect to each other

forming a cluster shape probably due to the interaction force among the long and thin nanowires. To better illustrate the structure, representative TEM images taken from the samples are given in Fig. 1e. The results show that the nanowires have an average diameter of 80 nm and the Ni-Co sulfides NWAs are highly porous and consist of numerous interconnected nanoparticles. As revealed in the high resolution TEM (HRTEM) image (Fig. 1f), a distinct set of interplanar spacings of 0.172, 0.210, 0.235 and 0.315 nm are visible. Besides, the typical diffraction rings in SAED pattern, together with the HRTEM images, demonstrates a polycrystalline nature of Ni-Co sulfides. The porous structure of the Ni-Co sulfides NWAs is also studied by the N_2 adsorption-desorption isotherm and pore size distribution (Fig. S1†). It is obvious that the mesoporous size of Ni-Co sulfides increased after ion-exchange compared with Ni-Co oxides. The pore size distribution within 1~4 nm of Ni-Co oxides dominated, however, the mesoporous size of Ni-Co sulfides was mainly in the range of 5~11 nm. Besides, Brunauer-Emmet-Teller (BET) specific surface area of the Ni-Co sulfides decreased after ion-exchange reaction (107 $m^2 g^{-1}$ and 15 $m^2 g^{-1}$ for Ni-Co oxides and sulfides, respectively). This can be explained by the growth of primary nanoparticles and the subsequent elimination of certain porosity after the S^{2-} ion exchange.

The successful preparation of Ni-Co oxides and Ni-Co sulfides are also suggested by XRD analysis as shown in Fig. 2a. Curve A is indexed to Ni-Co oxides with a Ni-Co molar ratio of 1 : 1. Since the Ni-Co oxides can be considered as cobalt oxides with some portion of cobalt substituted by nickel,[3] the XRD pattern of the mixed metal oxides precursor is very similar to that of pure CoO and NiO.[18] After

sulfurizing for 12 hours, four new peaks located at 30.9°, 37.5°, 49.7° and 54.9° appear (B curve), which take on a different pattern from that of Ni-Co oxides and are similar to the standard diffraction data of CoS (JCPDS no. 75-0605) and NiS (JCPDS no. 01-1286). All the diffraction peaks are weak and broad, indicating low crystallinity. This transformation and the surface composition of Ni-Co oxides and Ni-Co sulfides are further verified by X-ray photoelectron (XPS) analysis and the results are displayed in Fig. 2b-d. For Ni-Co oxides, the main peaks in Co 2p and Ni 2p spectrum are fitted with Co^{2+} and Ni^{2+} with corresponding two shakeup satellites, respectively.[18] Besides, no S 2p peaks is found in the spectrum of Ni-Co oxides. All the evidences above indicate the phase of nanowires on nickel foam is Ni-Co oxides before sulfuration. In the case of Ni-Co sulfides, the representative XPS spectram of Co 2p in Fig. 2b shows two major peaks with binding energies of 780.5 eV and 796.7 eV, respectively, in agreement with Co^{2+} of cobalt sulfide phase in the literature.[30] In Fig. 2c, two major peaks located at 855.7 eV and 873.5 eV for the same also can be observed in the region of Ni 2p, denoted as nickel in oxides/hydroxides to some extent as a result of exposure to ambient atomospher.[31,32] Meanwhile, the strong peaks at 161.7 eV in the region of S 2p, representative of the S^{2-} species in the composite, is consistent with typical values reported for CoS[30] and NiS.[33] The small peaks at 167.5 eV can be assigned to sulfur oxides at the surface of electrode.[34,35] Although there is a little deviation in peak position from pure CoS and NiS due to the synergistic effect of the two different metal sulfides in the composite, there is consistency in the results of XRD and XPS. As evidenced by both EDS and full XPS spectrum (Fig. S2†), the

sample contains mostly Co, Ni and S with only a trace presence of O, arising from the incomplete sulfuration, and the atomic ratio of Ni : Co : S : O is approximately 1 : 1 : 3.2 : 0.6.

In view of the facts above, we have reason to believe that the materials we fabricated in this article are mainly composed of Ni-Co sulfides and small amount of Ni-Co oxides instead of pure phases. For sake of simplicity, we still name it as Ni-Co sulfides.

Electrochemistry measurements

To explore the potential for the Ni-Co sulfides NWAs in supercapacitor, cyclic voltammetry (CV), galvanostatic charge-discharge tests were investigated. Fig. 3a shows the CV curves of the Ni-Co sulfides NWAs electrode in 1 M KOH aqueous electrolyte with various sweeping rates ranging from 1 mV s^{-1} to 20 mV s^{-1}. It is clear that a pair of redox peaks are visible in all CV curves, revealing distinct pseudo-capacitive characteristics which are associated with the Faradaic redox reactions related to M-O/M-O-OH, where M refers to Ni or Co.[36] With the increase of sweep rates, the current density increases and the positions of anodic and cathodic peaks shift to a more anodic and cathodic direction, respectively, indicating the fast redox reactions occur at electro-active material/electrolyte interface. And the linear relations of the square root of the scan rate dependence of the oxidation peak current at different scan rates (Fig. S3a†) demonstrates that it is a diffusion-controlled process.

Discharge profile of Ni-Co sulfides NWAs at various discharge current densities is exhibited in Fig. 3b. Note that the nickel foam itself has capacitive properties in alkaline solution and contribute a small percentage to capacitance.[37] So as to only evaluate the active materials' capacitance, we conducted experiment on a clean nickel foam under the same condition (Fig. S3b†) and the small contribution of bare nickel foam was subtracted according to calculation formula in literature.[38] Impressively, the Ni-Co sulfides NWAs electrode delivers high areal capacitance of 6.0, 5.1, 4.1, 3.5, 3.3 and 2.9 F cm^{-2} at the current density of 2.5, 5, 10, 15, 20 and 30 mA cm^{-2}, respectively. And the specific capacitance is 2415, 2053, 1627, 1403, 1312 and 1176 F g^{-1} at the corresponding current densities above. Preparation of electrodes with high mass loading of active materials plays crucial role in practical applications for supercapacitors. However, it is found that electrodes with high specific capacitance often suffer from drawbacks of extremely low mass loadings of the active material, along with the low areal capacitance.[4,9,39] But our electrodes afford trade-off between them, which result in high capacitive performance and exhibit both excellent areal capacitance and specific capacitance with high mass loading of active materials. Even at a high current density of 30 mA cm^{-2}, the electrodes still reveal a quite considerable capacitance of 2.9 F cm^{-2} (1176 F g^{-1}). To the best of our knowledge, the performance of Ni-Co sulfides obtained here is superior to the relevant data about cobalt/nickel sulfides[40-43] reported in literatures and some hybrid oxides/sulfides[3,6,9,11,21,24,44,45] nanocomposites, except the $NiCo_2S_4$ nanotube arrays[46] reported most recently. And it is even better than some core-shell cobalt oxides@cobalt/nickel

oxides/hydroxides[38,47,48] (Table S1†). The specific capacitance values as a function of applied current density of Ni-Co oxides and sulfides are displayed in **Fig. 3c**. In general, as the discharge current density increases, the specific capacitance decreases. The Ni-Co sulfides always deliver higher capacitance than Ni-Co oxides and there is still around 57% retention of its initial values (3.1 F cm^{-2}) for Ni-Co sulfides when current density increases from 5 mA cm^{-2} to 30 mA cm^{-2}.

As a fair comparison, the electrochemistry performance of the Ni-Co oxides NWAs obtained in the first synthesis process were also tested as electrode for supercapacitor and the results were plotted in Fig. 3d-f. Conspicuously, the CV curve integral area of Ni-Co sulfides is much larger and the peak current is almost as twice as that of Ni-Co oxides, implying higher electrochemical energy storage capacity. Fig. 3e shows the comparison of galvanostatic charge-discharge curves for the samples at current density of 5 mA cm^{-2}. The Ni-Co oxides and sulfides deliver a specific capacitance of 1222 F g^{-1} and 2053 F g^{-1}, and an areal capacitance of 2.2 F cm^{-2} and 5.1 F cm^{-2}, respectively. In strong contrast to Ni-Co oxides, the Ni-Co sulfides apparently demonstrate its prominent advantages in specific and areal capacitance as revealed by CV and galvanostatic charge-discharge measurements. To confirm these results, electrochemical impedance spectroscopy (EIS) tests were carried out at open circuit potential applying 5 mV ac voltage in the frequency range from 100 kHz to 0.01 Hz. The Nyquist plots of the Ni-Co oxides and sulfides electrodes are illustrated in Fig. 3f, with a fitted equivalent circuit (inset) and an enlarged view (inset). The impedance spectra are composed of three parts: the intersection on the real axis providing the

internal resistances of electrode (R_s), the semicircle at high frequency region corresponding to the charge-transfer resistance (R_{ct}) at the electrode/electrolyte interface and a linear part at low frequency representative of typical capacitor behavior. Of particular note, the charge transfer resistance (R_{ct}) of Ni-Co sulfides (0.8 Ω) is much smaller than that of Ni-Co oxides (1.5 Ω), which means easier electron transport. According to the N_2 adsorption-desorption results, the specific surface area of the Ni-Co sulfides NWAs decreases after ion-exchange reaction, however, the substitution of oxygen with sulfur might create a more flexible structure because the electronegativity of sulfur is lower than that of oxygen, which prevents the disintegration of the structure by the elongation between atoms and makes it easy for electrons to transport in the structure. Besides, the sulfur might act as a catalyst,[22] which invites further investigations. Furthermore, the line at low frequencies of the Ni-Co sulfides is closer to a parallel line along imaginary axis for an ideal capacitor. Therefore, the low charge-transfer resistance, together with its remarkable capacitive characteristic of Ni-Co sulfides NWAs enables faster redox reactions and easier electron transport, demonstrating that the Ni-Co sulfides electrodes are favorable for excellent electrochemistry performance which is in good accordance with the CV and galvanostatic charge-discharge results discussed above.

To evaluate the durability of the Ni-Co sulfides NWAs, current density dependence of the cycling performance (Fig. 3g) and charge-discharge cycling tests (Fig. 3h) at a constant current density of 15 mA cm^{-2} were employed to characterize its cycling performance. After successively cycling at various current densities, there is still

approximately 91% retention of its initial capacitance when it suddenly returns to 2.5 mA cm^{-2}. Moreover, the electrode retains a capacitance of 2.7 F cm^{-2} (1101 F g^{-1}) with 78.5% of the initial values after 3000 cycles. We researched on the causes of the decay through comparison of its morphology and impedance characteristic before and after 1000 cycling (Fig. S4†). As can be seen from the SEM images, the bottoms of some active materials are detached from the substrate, which displays the side views of the nanowires. However, the basic configuration of nanowires is preserved. In addition, the peel-off gives rise to both the higher internal resistance and the charge-transfer resistance (Fig. S4c† and Table S2†). Given the discussed aforementioned, we can conclude that the decline of the performance upon cycling is mainly ascribed to the weak adhesion between active materials and substrate, rather than the defect of the materials, *i.e.*, in terms of its outstanding intrinsic electrochemical capacitance properties, the Ni-Co sulfides NWAs are a promising material for application in supercapacitor.

To further assess the application value of the Ni-Co sulfides NWAs, an asymmetric supercapacitor was fabricated which the Ni-Co sulfides NWAs were used for the positive electrode and the commercial activated carbon was used as the negative electrode. The electrochemistry test results were exhibited in Fig. 4. Based on the three-electrode electrochemical measurements of both Ni-Co sulfides and AC electrodes (Fig. S5a†), certain mass of AC supported on Ni foam was chosen to balance the two electrodes' capacitance.[28,49] CV curves of the asymmetric capacitor at different potential window (Fig. S5b†) shows that the cell voltage could be extended to 1.8 V. CV curves in Fig. 4b at different scan rates exhibit electrical double layer

capacitance and pseudocapacitance from AC and Ni-Co sulfides electrodes, respectively. Galvanostatic charge-discharge tests (Fig. 4c) were employed to calculate the energy density and power density of the supercapacitor and Ragone plot at different current densities was obtained (Fig. 4d). An energy density of 25 Wh kg^{-1} is achieved at the power density of 447 W kg^{-1} and still remains 17.8 Wh kg^{-1} at high power density of 3.57 kW kg^{-1}, which demonstrates its superiority in retention of energy density. Fig. 4e reveals the cycling life and coulomb efficiency of the asymmetric supercapacitor. As can be seen, the cell capacitance mainly decays in the first ~1000 cycling, which is due to the weak adhesion between active materials and substrate discussed above, and stays stable afterwards. Furthermore, we assembled two supercapacitors in series and powered a 3 mm diameter red (2.0 V, 20 mA) round light-emitting diode (LED) indicator (Fig. 4f and g). The LED stayed alight for more than 30 minutes after charging separately for a total time of 6 min. These results further demonstrated the practical application merit of the Ni-Co sulfides NWAs described in this work.

Conclusion

In summary, we adopted a facile two-step hydrothermal method to prepare Ni-Co sulfides nanowires arrays on Ni foam for the application in supercapacitor. The electrochemistry tests show that the electrode exhibits high specific capacitance of 2415 F g^{-1} and pronounces areal capacitance of 6.0 F cm^{-2} at current density of 2.5 mA cm^{-2}, as well as good rate capability and cycle performance (78.5% retention after 3000 cycles), which outperforms the electrochemistry performance of Ni-Co oxides synthesized from the first step. The enhancement is probably ascribed to the catalytic

nature of sulfur element and easier and faster ion/electron diffusion after ion exchange. Furthermore, an asymmetric supercapacitor delivers an energy density of 17.8 Wh kg^{-1} at a high power density of 3.57 kW kg^{-1}. All the evidences suggest the Ni-Co sulfides NWAs have a great potential used as a high-performance supercapacitor and can be possibly applied to various applications involving chemical and energy transformation processes.

Acknowledgment

This work was supported by the sharing of Chongqing University's large-scale equipment

Notes and references

1 P. Simon and Y. Gogotsi, *Nat. Mater.*, 2008, **7**, 845.

2 J. R. Miller and P. Simon, *Science*, 2008, **321**, 651.

3 H. B. Wu, H. Pang and X. W. Lou, *Energy Environ. Sci.*, 2013, **6**, 3619.

4 T.-Y. Wei, C.-H. Chen, H.-C. Chien, S.-Y. Lu and C.-C. Hu, *Adv. Mater.*, 2010, **22**, 347.

5 L. F. Hu, L. M. Wu, M. Y. Liao, X. H. Hu and X. S. Fang, *Adv. Funct. Mater.*, 2012, **22**, 998.

6 H. Jiang, J. Ma and C. Z. Li, *Chem. Commun.*, 2012, **48**, 4465.

7 Q. F. Wang, B. Liu, X. F. Wang, S. H. Ran, L. M. Wang, D. Chen and G. Z. Shen, *J. Mater. Chem.*, 2012, **22**, 21647.

8 J. W. Xiao and S. H. Yang, *RSC Adv.*, 2011, **1**, 588.

9 C. Z. Yuan, J. Y. Li, L. R. Hou, X. G. Zhang, L. F. Shen and X. W. Lou, *Adv. Funct. Mater.*, 2012, **22**, 4592.

10 G. Q, Zhang and X. W. Lou, *Adv. Mater.*, 2013, **25**, 976.

11 G. Q. Zhang, H. B. Wu, H. E. Hoster, M. B. Chan-Park and X. W. Lou, *Energy Environ. Sci.*, 2012, **5**, 9453.

12 Q. F. Wang, X. F. Wang, B. Liu, G. Yu, X. J. Hou, D. Chen and G. Z. Shen, *J. Mater. Chem. A*, 2013, **1**, 2468.

13 G. Q. Zhang and X. W. Lou, *Sci. Rep.*, 2013, DOI: 10.1038/srep01470.

14 R. B. Rakhi, W. Chen, D. Cha and H. N. Alshareef, *Nano Lett.*, 2012, **12**, 2559.

15 J. P. Liu, J. Jiang, C. W. Cheng, H. X. Li, J. X. Zhang, H. Gong and H. J. Fan, *Adv. Mater.*, 2011, **23**, 2076.

16 C. Z. Yuan, L. Yang, L. R. Hou, L. F. Shen, X. G. Zhang and X. W. Lou, *Energy Environ. Sci.*, 2012, **5**, 7883.

17 G. P. Felcher and Y. Y. Huang, *J. Magn. Magn. Mater.*, 1993, **121**, 105.

18 F. Yang, J. Y. Yao, F. L. Liu, H. C. He, M. Zhou, P. Xiao, Y. H. Zhang, *J. Mater. Chem. A*, 2013, **1**, 594.

19 C.-H. Lai, M.-Y. Lu and L.-J. Chen, *J. Mater. Chem.*, 2012, **22**, 19.

20 M.-R. Gao, Y.-F. Xu, J. Jiang and S.-H. Yu, *Chem. Soc. Rev.*, 2013, **42**, 2986.

21 H. C. Chen, J. J. Jiang, L. Zhang, H. Z. Wan, T. Qi and D. D. Xia, *Nanoscale*, 2013, **5**, 8879.

22 S. H. Park, Y.-K. Sun, K. S. Park, K. S. Nahm, Y. S. Lee, M. Yoshio, *Electrochim. Acta*, 2002, **47**, 1721.

23 H. Z. Wan, J. J. Jiang, J. W. Yu, K. Xu, L. Miao, L. Zhang, H. C. Chen and Y. J. Ruan, *CrystEngComm*, 2013, **15**, 7649.

24 S. J. Peng, L. L. Li, C. C. Li, H. T. Tan, R. Cai, H. Yu, S. Mhaisalkar, M. Srinivasan, S. Ramakrishna and Q. Y. Yan, *Chem. Commun.*, 2013, **49**, 10178.

25 Z. H. Wang, L. Pan, H. B. Hu and S. P. Zhao, *CrystEngComm*, 2010, **12**, 1899.

26 C.-W. Kung, H.-W. Chen, C.-Y. Lin, K.-C. Huang, R. Vittal and K.-C. Ho, *ACS Nano*, 2012, **6**, 7016.

27 Y. Wang, Q. S. Zhu, L. Tao and X. W. Su, *J. Mater. Chem.*, 2011, **21**, 9248.

28 Z. J. Fan, J. Yan, T. Wei, L. J. Zhi, G. Q. Ning, T. Y. Li and F. Wei, *Adv. Funct. Mater.*, 2011, **21**, 2366.

29 H. Pang, J. W. Deng, J. I. Du, S. J. Li, J. Li, Y. H. Ma, J. S. Zhang and J. Chen,

Dalton Trans., 2012, **41**, 10175.

30 J.-Y. Lin and S.-W. Chou, *RSC Adv.*, 2013, **3**, 2043.

31 A. N. Buckley, *J. Appl. Electrochem.*, 1991, **21**, 575.

32 F. Loglio, M. Innocenti, A. Jarek, S. Caporali, I. Pasquini, M. L. Foresti, *J. Electroanal. Chem.*, 2010, **638**, 15.

33 S.-C. Han, H.-S. Kim, M.-S. Song, P. S. Lee, J.-Y. Lee, and H.-J. Ahn, *J. Alloys Compd.*, 2003, **349**, 290.

34 A. Galtayries, C. Cousi, S. Zanna and P. Marcus, *Surf. Interface Anal.*, 2004, **36**, 997.

35 Y.-M. Sun, D. Sloan, D. J. Alberas, M. Kovar, Z.-J. Sun and J. M. White, *Surf. Sci.*, 1994, **319**, 34.

36 H. L. Wang, Q. M. Gao and L. Jiang, *Small*, 2011, **7**, 2454.

37 W. Xing, S. Z. Qiao, X. Z. Wu, X. L. Gao, J. Zhou, S. P. Zhuo, S. B. Hartono and D. Hulicova-Jurcakova, *J. Power Sources*, 2011, **196**, 4123.

38 C. Guan, J. P. Liu, C. W. Cheng, H. X. Li, X. L. Li, W. W. Zhou, H. Zhang and H. J. Fan, *Energy Environ. Sci.*, 2011, **4**, 4496.

39 J.-K. Chang, C.-M. Wu and I.-W. Sun, *J. Mater. Chem.*, 2010, **20**, 3729.

40 J. Xu, Q. F. Wang, X. W. Wang, Q. Y. Xiang, B. Liang, D. Chen and G. Z. S, *ACS Nano*, 2013, **7**, 5453.

41 Q. H. Wang, L. F. Jiao, H. M. Du, Y. C. Si, Y. J. Wang and H. T. Yuan, *J. Mater. Chem.*, 2012, **22**, 21387.

42 T. Zhu, Z. Y. Wang, S. J. Ding, J. S. Chen and X. W. Lou, *RSC Adv.*, 2011, **1**, 397.

43 S.-W. Chou and J.-Y. Lin, *J. Electrochem. Soc.*, 2013, **160**, D178.

44 M.-C. Liu, L.-B. Kong, C. Lu, X.-M. Li, Y.-C. Luo and L. Kang, *ACS Appl. Mater. Interfaces*, 2012, **4**, 4631.

45 J.-H. Zhong, A.-L. Wang, G.-R. Li, J.-W. Wang, Y.-N. Ou and Y.-X. Tong, *J. Mater. Chem.*, 2012, **22**, 5656.

46 Chen, H.; Jiang, J.; Zhang, L.; Xia, D.; Qi, T.; Wan, H.. *J. Power Sources*, 2013, DOI: 10.1016/j.jpowsour.2013.12.092.

47 X. H. Xia, J. P. Tu, Y. Q. Zhang, J. Chen, X. L. Wang, C. D. Gu, C. Guan, J. S. Luo and H. J. Fan, *Chem. Mater.*, 2012, **24**, 3793.

48 X. H. Xia, J. P. Tu, Y. Q. Zhang, X. L. Wang, C. D. Gu, X.-B. Zhao and H. J. Fan, *ACS Nano*, 2012, **6**, 5531.

49 Y. W. Cheng, H. B. Zhang, C. V. Varanasi and J. Liu, *Energy Environ. Sci.*, 2013, **6**, 3314.

50 H. L. Wang, C. M. B. Holt, Z. Li, X. H. Tan, B. S. Amirkhiz, Z. W. Xu, B. C. Olsen, T. Stephenson and D. Mitlin, *Nano Res.*, 2012, **5**, 605.

51 Y.-M. Wang, X. Zhang, C.-Y. Guo, Y.-Q. Zhao, C.-L. Xu and H.-L. Li, *J. Mater.*

Chem. A, 2013, **1**, 13290.

52 X. Sun, G. K. Wang, H. T. Sun, F. Y. Lu, M. P. Yu and J. Lian, *J. Power Sources*, 2013, **238**, 150.

Figure captions

Fig. 1 (a) Schematic illustration of the synthesis processes. (b) Optical image of Ni foam, Ni-Co oxides and Ni-Co sulfides NWAs. (c and d) SEM images of Ni-Co sulfides NWAs with different magnifications. Inset in (d) is the locally enlarged image. (e) TEM images of a single Ni-Co sulfides nanowire scratched off the Ni foam. (f) HRTEM image and (g) the corresponding SAED pattern of the Ni-Co sulfides nanowire.

Fig. 2 (a) XRD pattern of the Ni-Co oxides and Ni-Co sulfides. XPS spectra of (b) Co 2p, (c) Ni 2p and (d) S 2p for Ni-Co oxides and Ni-Co sulfides.

Fig. 3 (a) CV curves of the Ni-Co sulfides NWAs at different scan rates. (b) Galvanostatic discharge plots of the Ni-Co sulfides NWAs at different current densities. (c) The corresponding specific capacitance of Ni-Co oxides and sulfides as a function of current density. (d) CV curves of Ni-Co oxides and sulfides at scan rate of 5 mV s^{-1}. (e) Galvanostatic charge-discharge curves of the Ni-Co oxides and sulfides at current density of 5 mA cm^{-2}. (f) EIS Nyquist plots of the Ni-Co oxides and sulfides. The insets are the corresponding equivalent circuit and the partial enlarged Nyquist plots. (g) Current density dependence of the cycling performance of Ni-Co sulfides NWAs electrode. (f) Cycling performance of Ni-Co sulfides NWAs electrode at current density of 15 mA cm^{-2}. The inset is the last 16 cycles.

Fig. 4 (a) Schematic illustration of the asymmetric supercapacitor configuration. (b) CV curves of the asymmetric supercapacitor at different scan rates. (c) Galvanostatic discharge curves of the asymmetric supercapacitor at different current densities. (d) Ragone plot of our supercapacitor device compared with other data. (e) Cycling performance and coulomb efficiency of our device. (f) A photograph of a red LED lighted up by two supercapacitors in series. (g) Photographs of the red LED at different stages.

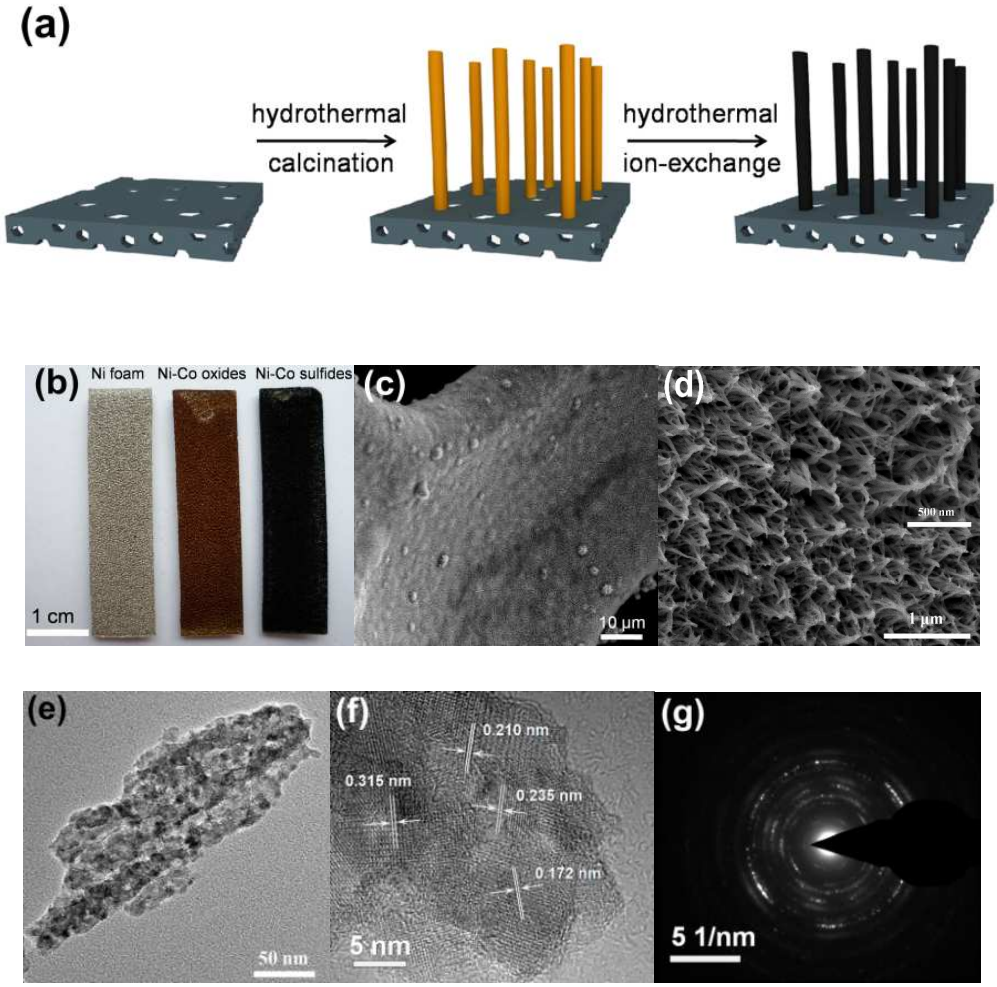

Fig. 1

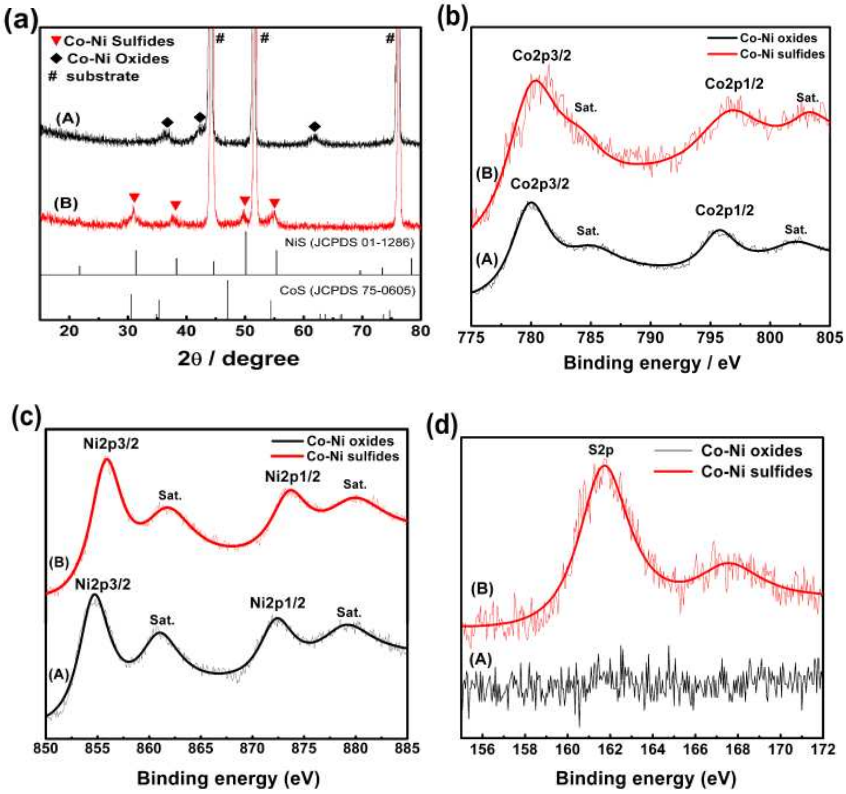

Fig. 2

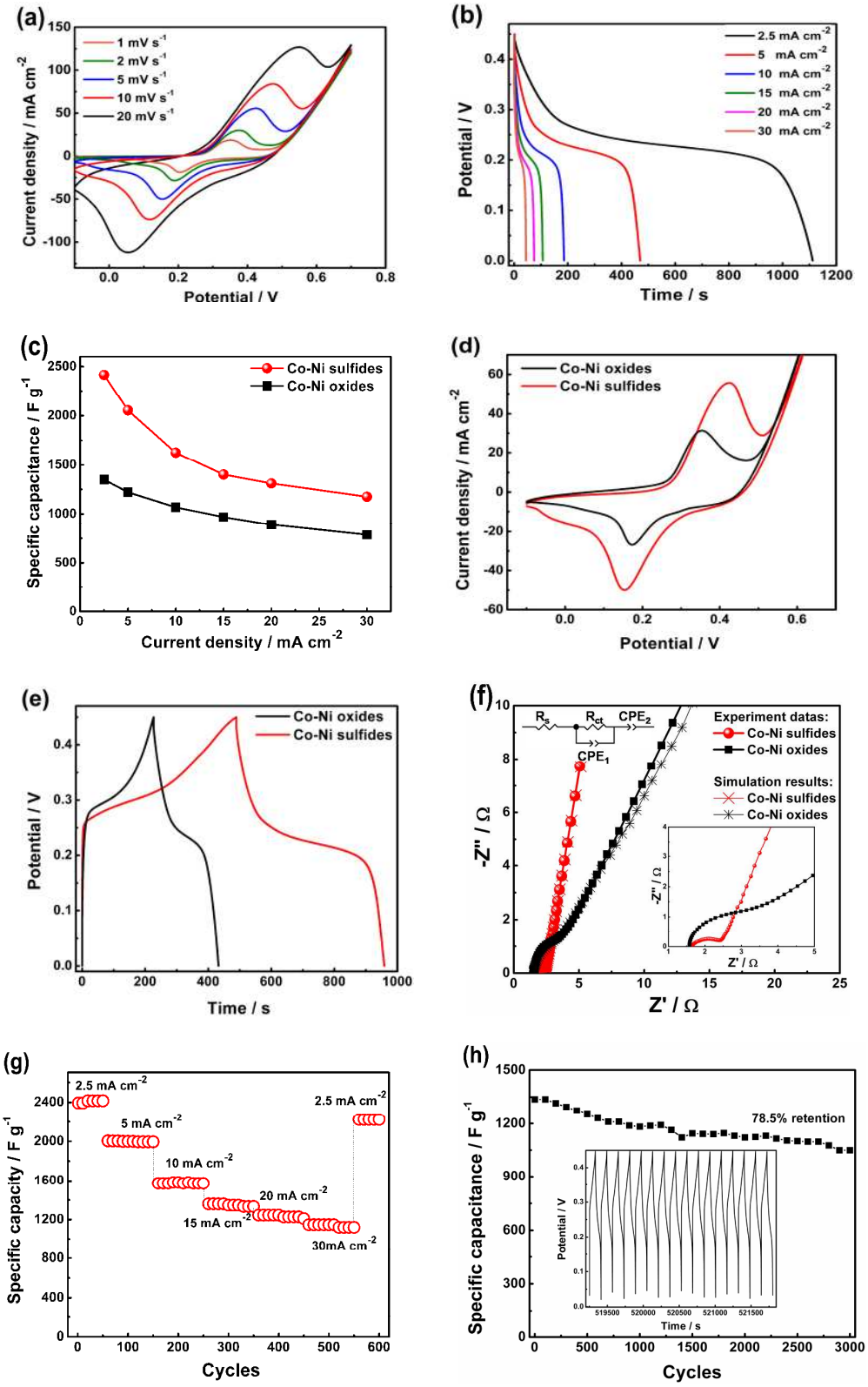

Fig. 3

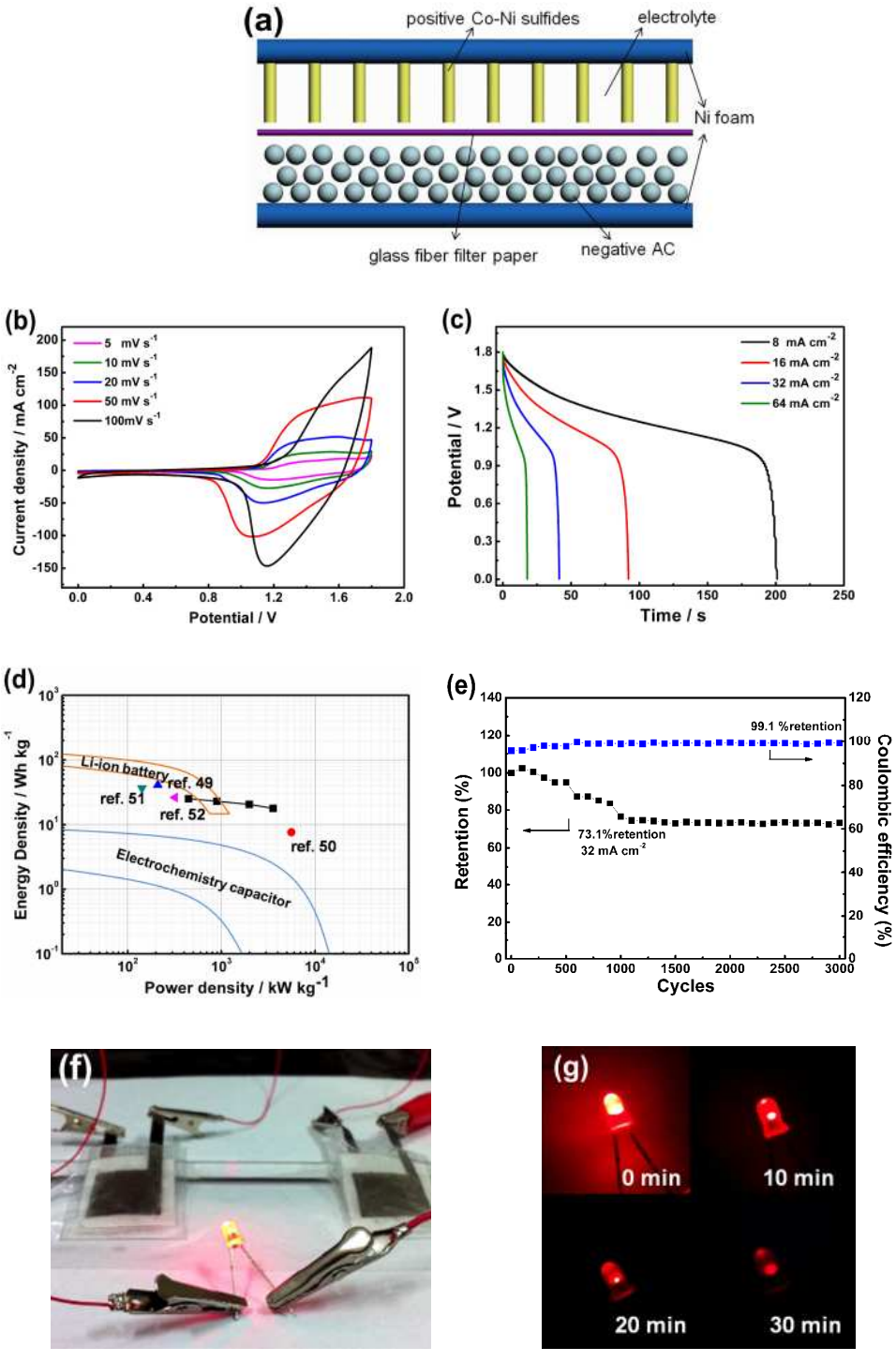

Fig. 4

Ni-Co sulfides nanowires synthetized by a two-step hydrothermal method show good performance when serve as positive electrode for asymmetric supercapacitor.